AD-A145 868 SELECTIVE OBSERVATION OF ELASTIC-BODY RESONANCES VIA THEIR RINGING IN TRA..(U) CATHOLIC UNIV OF AMERICA WASHINGTON DC DEPT OF PHYSICS W E HOWELL ET AL. 1/1

UNCLASSIFIED 12 SEP 84 N00014-76-C-0430 F/G 20/1 NL

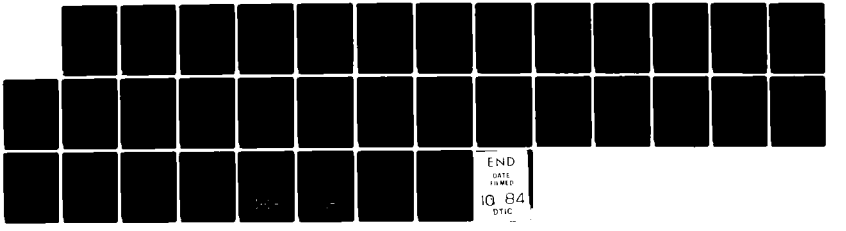

END
DATE FILMED
10 84
DTIC

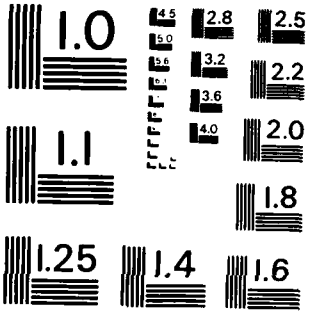

MICROCOPY RESOLUTION TEST CHART
NATIONAL BUREAU OF STANDARDS - 1963 - A

Selective Observation of Elastic-Body Resonances Via their Ringing in Transient Acoustic Scattering

W. E. Howell and S. K. Numrich
Naval Research Laboratory
Washington, DC 20375

Herbert Überall
Naval Research Laboratory
Washington, DC 20375, and
Department of Physics, Catholic University of America
Washington, DC 20064

DEPARTMENT OF PHYSICS

The Catholic University of America

Washington, D.C. 20064

Approved for public release; distribution unlimited.

Selective Observation of Elastic-Body Resonances Via their Ringing in Transient Acoustic Scattering

W. E. Howell and S. K. Numrich
Naval Research Laboratory
Washington, DC 20375

"
Herbert Überall
Naval Research Laboratory
Washington, DC 20375, and
Department of Physics, Catholic University
of America
Washington, DC 20064

Abstract

An elastic body immersed in a fluid will ring when isonified by sound whose frequency is the same as one of the resonances of that body. Correspondence has been established between these normal mode resonances of the body and the individual circumferential waves predicted by creeping wave theory. Insonifying the target by a relatively long sinusoidal wave train, with a narrow spectrum centered around, or away from, a selected resonance frequency, results in a series of superimposed responses consisting of the specular reflection and succession of creeping waves arriving after repeated circumnavigations of the body which, at resonance only, add in phase to generate the ringing response. Echoes from spherical targets are analyzed in this fashion, and are also associated with the resonance poles in the complex frequency plane, obtained by us in the form of contour plots.

Unclassified

SECURITY CLASSIFICATION OF THIS PAGE (When Data Entered)

REPORT DOCUMENTATION PAGE	READ INSTRUCTIONS BEFORE COMPLETING FORM
1. REPORT NUMBER	2. GOVT ACCESSION NO. 3. RECIPIENT'S CATALOG NUMBER
4. TITLE (and Subtitle) Selective Observation of Elastic-Body Resonances via their Ringing in Transient Acoustic Scattering	5. TYPE OF REPORT & PERIOD COVERED Technical Report (interim Oct.1,1983 - Sept.30,1984 6. PERFORMING ORG. REPORT NUMBER
7. AUTHOR(s) W. E. Howell, S. K. Numrich and H. Uberall	8. CONTRACT OR GRANT NUMBER(s) ONR N00014-76-C-0430
9. PERFORMING ORGANIZATION NAME AND ADDRESS Department of Physics Catholic University Washington, DC 20064	10. PROGRAM ELEMENT, PROJECT, TASK AREA & WORK UNIT NUMBERS Program 61153M, Project RR011-08, Task RR011-008-001 Work Unit NR 384-914
11. CONTROLLING OFFICE NAME AND ADDRESS Office of Naval Research Physics Program Arlington, VA 22217	12. REPORT DATE September 12, 1984 13. NUMBER OF PAGES 23pp+8pp figs.+2pp Form1473
14. MONITORING AGENCY NAME & ADDRESS (if different from Controlling Office)	15. SECURITY CLASS. (of this report) Unclassified 15a. DECLASSIFICATION/DOWNGRADING SCHEDULE

16. DISTRIBUTION STATEMENT (of this Report)

Approved for public release; distribution unlimited.

17. DISTRIBUTION STATEMENT (of the abstract entered in Block 20, if different from Report)

18. SUPPLEMENTARY NOTES

19. KEY WORDS (Continue on reverse side if necessary and identify by block number)

Acoustic scattering, elastic target, long sound pulses, ringing of resonances.

20. ABSTRACT (Continue on reverse side if necessary and identify by block number)

An elastic body immersed in a fluid will ring when isonified by sound whose frequency is the same as one of the resonances of that body. Correspondence has been established between these normal mode resonances of the body and the individual circumferential waves predicted by creeping wave theory. Insonifying the target by a relatively long sinusoidal wave train, with a narrow spectrum centered around, or away from, a selected resonance frequency, results in a series of superimposed responses consisting of the

DD FORM 1 JAN 73 1473 EDITION OF 1 NOV 65 IS OBSOLETE

S/N 0102-LF-014-6601

SECURITY CLASSIFICATION OF THIS PAGE (When Data Entered)

specular reflection and succession of creeping waves arriving after repeated circumnavigations of the body which, at resonance only, add in phase to generate the ringing response. Echoes from spherical targets are analyzed in this fashion, and are also associated with the resonance poles in the complex frequency plane, obtained by us in the form of contour plots.

A-1

I. Introduction

The ringing of resonances in sound scattering experiments from elastic cylinders and spheres has first been mentioned by Faran[1]. In the computational results for scattered sound pulses obtained by Hickling[2], ringing effects are evident but have not been discussed by him. Subsequent studies of pulse scattering from rigid spheres by Rudgers[3], or from elastic cylinders by Veksler[4], observed theoretically certain transient effects in the backscattering of long pulses, interpreting them as a coherent superposition of echo pulses specularly returned from the target, and circumferential surface waves arising after successive circumnavigations. (For rigid spheres, these surface waves are exclusively of external, or "creeping" type, while for elastic bodies they are predominantly internal[5]).

A recent series of experimental studies on elastic cylinders by Ripoche et al.[6,7] has been devoted to the measurement of transients as they occur in the scattering of long incident pulses. Together with theoretical analysis[8], these studies have developed the "Method of Isolation and Identification of Resonances (MIIR)" in which the transients trailing the main reflected pulse at a resonance frequency (i.e., the "ringing"), but absent off resonance, have been employed as a highly sensitive means for obtaining the resonance spectrum of elastic cylinders or shells, thus contributing significantly to the emerging technology on the classification of submerged targets[9].

Previous work by one of the present authors and collaborators[10-13] on transient scattering from a sphere has shown, for the case of short incident pulses, how the scattering amplitude can be expressed as a residue series over its complex-frequency poles, the latter representing the resonant eigenfrequencies of the target. The broad spectrum of a short pulse, stretching over many poles, necessitated the inclusion of a large number of residues in the mentioned calculation. By employing a long pulse with a spectrum narrower than the spacing between poles, however, it is possible to selectively excite a given resonance by choosing the carrier frequency to coincide with the resonance frequency, or not to excite it by choosing a carrier frequency different from a resonance frequency. As a consequence, and as demonstrated by Ripoche's work[6-8], it is possible to excite one resonance at a time, a procedure which may be employed for target identification purposes[8,14].

In the present work, we study the excitation of elastic-sphere resonances by long sinusoidal wave trains, and investigate how the initial and final transients in the echo which appear near a resonance frequency can be interpreted by multiply-circumnavigating circumferential wave trains. The relation of initial transients, and of the interference of reflected and circumnavigating pulses, to the acoustic form function of the target is established. In this connection, we also obtain contour plots of the scattering function in the complex frequency planes (an

extension of the form function into the complex domain) for aluminum, tungsten carbide, and lucite spheres which greatly aid in the understanding of the real-frequency form function, and of the transient effects appearing in the returned pulse trains.

II. Steady State Theory, and Pole Contour Diagrams

Theoretical expressions for the acoustic scattering amplitude from an elastic sphere have been given in the literature[15]. A plane wave

$$p_{inc} = e^{i(kz-\omega t)} \tag{1}$$

incident on an elastic sphere of radius a centered at the origin, with $k = \omega/c$, leads to a far-field backscattering amplitude

$$p_{sc} = (a/2r)e^{i(kr-\omega t)} f(x), \tag{2}$$

with a form function

$$f(x) = \sum_{n=1}^{\infty} f_n(x), \tag{3a}$$

$$f_n(x) = (4/ix)(-1)^n (n+\tfrac{1}{2}) B_n, \tag{3b}$$

where $x = ka$ denotes the non-dimensional frequency of sound in the ambient fluid.

The coefficients B_n are given by

$$B_n = \frac{A_1(d_{22}d_{33} - d_{32}d_{23}) - A_2(d_{12}d_{33} - d_{32}d_{13})}{d_{11}(d_{22}d_{33} - d_{32}d_{23}) - d_{21}(d_{12}d_{33} - d_{32}d_{13})}, \tag{4a}$$

where

$$
\begin{aligned}
d_{11} &= (\rho/\rho_s)\, z^2 h_n^{(1)\prime}(x), \\
d_{12} &= [2n(n+1) - z^2]\, j_n(y) - 4y\, j_n'(y), \\
d_{13} &= 2n(n+1)[2 j_n'(z) - j_n(z)], \\
d_{21} &= -x\, h_n^{(1)\prime}(x), \\
d_{22} &= y\, j_n'(y), \\
d_{23} &= n(n+1)\, j_n(z), \\
d_{32} &= 2[j_n(y) - y\, j_n'(y)], \\
d_{33} &= 2z\, j_n'(z) + [z^2 - 2n(n+1) + 2]\, j_n(z), \\
A_1 &= -(\rho/\rho_s)\, z^2 j_n(x), \\
A_2 &= x\, j_n'(x),
\end{aligned}
\tag{4b}
$$

and where $j_n(x)$ are the spherical Bessel functions, and $h_n^{(1)}$ the spherical Hankel functions of first kind.

Here, ρ and ρ_s denote the densities of the surrounding fluid (which will be taken as water with $\rho = 1\, gm/cm^3$ and of the sphere, respectively; further, $y = (c_\ell/c)\, x$ and $z = (c_s/c)\, x$ contain the longitudinal and shear speeds c_ℓ, c_s, of the sphere material, respectively

Form functions have been calculated as a function of real frequency for tungsten carbide, aluminum, and lucite spheres using the material parameters shown in Table I. In addition, the values of $|f(x)|$ were also obtained in the form of contour plots over a region of the complex-x plane. Our results are displayed in Figs. 1-3, showing in the top portion the form function modulus $|f(x)|$ plotted over the real frequency axis, and in the bottom portion contour plots of $|f(x)|$ over the complex frequency plane. Figure 1 refers to tungsten carbide, Fig. 2 to aluminum, and Fig. 3 to lucite. While the form function plots for real x of spheres of these materials are well-known, our contour plots reveal important new aspects of $|f(x)|$. Analogous contour plots were also obtained for the case of radar scattering[16,17].

The dark areas of the figures denote large values of $|f(x)|$, and contain the poles of the form function. The three prominent pole chains, converging in the lower-left corners of Figs. 1-3, are due to the resonances of external (Franz, or creeping) surface waves as they span the sphere's circumference with successively increasing (half-) integer numbers of wavelengths[10-12]. Above the least-damped (i.e., having smallest imaginary parts) Franz-pole (F) chain one recognizes in Figs. 1 and 2 a much more widely spaced chain of much narrower poles corresponding to the Rayleigh wave[18], an internal surface wave with speed comparable to the bulk wave speeds in the material,

faster than that of the Franz waves (hence the wider spacing). For lucite (Fig. 3), the identification of the Rayleigh (R) poles is less unambiguous, since several pole chains crowd here close to the real frequency axis. In fact, further pole chains (closer to the real axis) are also contained in Figs. 1 and 2, but are hardly visible, since these poles [which are due to Whispering-Gallery (WG) wave resonances] are so narrow that they have often not been registered by our contouring procedure. Examples of these are given in Fig. 10 of Reference 15; in addition, Fig. 4 shows a blow-up of the contour diagram of Fig. 1 (tungsten carbide) between x = 13.3 and 14.3 in which a Rayleigh pole (lower right) and a WG pole (upper left) are both visible, together with the interference features they cause in the form function.

It is interesting to see from Figs. 1-4 that every R and WG pole seems to be accompanied by a zero in the form function (contained in the white areas), while for F poles, such an association is not strictly one-to-one, apparently. Extrapolating all these contour diagrams to the real axis results in the form function plots of Figs. 1-4 (top). The interference features of these have been analyzed earlier[18], but they now become more easily understandable by comparison with the contour plots. The deep minima in the form function are evidently due to the R-zeros (rather than the R-poles themselves), and the narrow interferences are due to the WG zeros and/or poles. The physical origin of these interferences can be attributed[18] to the destructive interference

of the R-wave echoes with a specularly-reflected echo (see also an analogous effect in the reflection of sound from fluid layers[19]), while in the case of a lucite sphere (Fig. 3), the presence of peaks rather than interference minima in the form function can be seen from the associated contour plot to be due to the greater closeness of a pole chain to the real axis, rather than that of its accompanying zeros.

III. Theory of Transients, and Numerical Results

An incident plane-wave pulse can be represented by the Fourier integral

$$p_{inc}(z,t) = \int G(k) e^{ik(z-ct)} dk/2\pi \ . \tag{5}$$

A sinusoidal wave train

$$p_{inc}(z=0,t) = \begin{cases} \sin \omega_0 t & 0 \le t \le t_p, \\ 0 & \text{elsewhere} \end{cases} \tag{6a}$$

with carrier frequency ω_0 and time duration t_p has a spectrum

$$\frac{1}{a} G(k) = \frac{1-e^{i(x+x_0)\tau_p}}{2(x+x_0)} - \frac{1-e^{i(x-x_0)\tau_p}}{2(x-x_0)} \ , \tag{6b}$$

where we designate $\tau_p = ct_p/a$, $x_0 = a\omega_0/c$. Introducing backscattered form functions $\tilde{f}(x)$ and $\tilde{f}_n(x)$ by

$$\tilde{f}(x) = \sum_{n=1}^{\infty} \tilde{f}_n(x), \tag{7a}$$

$$\tilde{f}_n(x) = e^{i(kr-\omega t)} f_n(x), \tag{7b}$$

results in the expressions for the pulsed case:

$$\tilde{f}(\tau) = \sum_{n=1}^{\infty} \tilde{f}_n(\tau), \tag{8a}$$

$$\tilde{f}_n(\tau) = (-1)^n \frac{2n+1}{i\pi a} \int G(k) B_n(k) e^{-ix\tau} \, dx/x, \tag{8b}$$

where we have introduced a non-dimensional time variable $\tau = (ct-r)/a$. In the calculations to follow, Eqs. (8) were evaluated using numerical integration.

Figure 5 shows in the center part an incident pulse train, having a length $\tau_p = 25$ (i.e., covering a length of 25 radii), and a carrier frequency $x_o = 14.07$. The top portion of the figure depicts its spectrum, G(x), superimposed on the form function $|f(x)|$ of a tungsten carbide sphere. We chose x_o to coincide with the deep minimum of $|f(x)|$ caused by the R-zero of Fig. 4. The bottom portion of the figure shows the scattered pulse; it arrives at the observer at $\tau = -2$, this being due to its reflection at the vertex of the sphere which the incident pulse reaches before it attains the plane through the center

of the sphere, z = 0. After an initial transient, the scattered pulse reaches a strongly constricted quasi-"steady-state" amplitude with the constriction being due to the fact that the steady-state form function $|f(x)|$ has a deep minimum at the selected center frequency x_o. After a duration of 25 units of τ (equal to that of the incident pulse), the scattered signal shoots up to its original value, and from there on it consists of a slowly decaying final transient that can be attributed to the ringing of the R-pole at x = 14.07, which has thus been selectively excited by our incident pulse. Note that in Hickling's study[2], the steady-state amplitude had been associated with interference features in the form function, but he did not discuss initial or final transients, clearly visible in his results.

In Fig. 6, the incident pulse has been shifted to a center frequency of x_o=13.7, i.e. in between the R- and the WG- pole (see Fig. 4). Since here the form function is close to its normal level ($\sim$1) between two resonances, the scattered pulse has a shape close to that of the incident pulse, apart from slight initial transients and a slight tail. This residual ringing is probably due to the overlap of the first sidelobe of G(x) with the x_o=14.07 R-pole (it has the same decay constant as the ringing in Fig. 5); had we chosen an incident pulse with a narrower spectrum (as was the case in the Ripoche experiments[6-8]), this ringing should have been completely absent here.

Closer inspection of the tail in Fig. 5 (and also Fig. 6) reveals that it contains a series of descending steps; this is demonstrated in Fig. 7 which represents a blow-up of the initial (top) and final (bottom) transient regions of Fig. 5 (with the τ- scale displaced again so that the pulse starts at $\tau = 0$). Veksler[4] has found and discussed these steps previously, but they are also visible in earlier experimental long-pulse scattering results by Neubauer et al.[20].

IV. Physical Interpretation

The physical situation is best discussed using the schematic graph of Fig. 8. The large rectangle denotes the envelope of a rectangular incident pulse (as in the center portion of Figs. 5,6), which essentially coincides with the shape of the specularly reflected pulse, due to minimal dispersion of the specularly reflected wave[21]. As discussed above, the head of this specular pulse arrives at the observer at $\tau = -2$. The dotted rectangles indicate further wave trains that penetrate the sphere, get reflected from its rear backside vertex, and reach the observer with short time delays (due to the high interior sound speeds) after a possible series of back-and-forth bounces with ever-decreasing amplitude, as indicated. These interior reflections will not be our concern here. In addition, there will also be present circumferentially-traveling wave trains with rectangular shapes not too different from that of the incident pulse (in spite of some dispersion[10-12]), which, for backscattering, proceed to the observer after 1/2, 3/2, 5/2...

circumnavigations of the sphere's circumference, with successively decreasing amplitudes (due to radiation loss) as indicated in Fig. 8 (small solid rectangles). Their successive arrival times are at $\tau = \pi$, 3π, 5π ..., multiplied by the ratio of external and surface wave speeds, as shown.

Actually, there exists a large number of such surface waves (R,WG) which in general, after each circumnavigation, are out of phase with each other, so that the overlap of their rectangles in Fig. 8 will effectively cancel their contribution. However, if the carrier frequency coincides with an eigenfrequency of the sphere, which corresponds to a certain surface wave producing a phase match with itself after each circumnavigation[18], then all the successive circumferential wavetrains in Fig. 8 corresponding to <u>that</u> surface wave (only) will add in phase. This leads to a step-wise decaying tail in region (iii) of Fig. 8 which represents the ringing of the resonance at the frequency in question, but also to an initial transient in region (i) of Fig. 8, stepped similarly as the final transient (tail), in which the successively arriving circumferential wave heads also add in phase. It now depends whether the resonance in question interferes with the specularly reflected wave destructively (the more usual case for metal targets) or constructively: in the first case, there will be a descending staircase in region (i) of the reflected signal leading down to the reduced steady-state amplitude of regior (ii), as is clearly evident in the bottom portion of Fig. 5.

In the second case, the initial transients (i) will form an ascending staircase leading to an augmented steady-state amplitude in region (ii), as e.g. in the center portions of Figs. 17 and 18 of Reference 2. The bottom portion of our Fig. 6 represents an in-between situation, with some augmentation visible.

Figure 8 shows that the width of the steps is given by

$$\Delta\tau = 2\pi c/c_\ell \ . \tag{9a}$$

Resonances originate if, for the case of the sphere, a half-integer number of wavelengths[22] λ_ℓ of the lth surface wave span the circumference of the sphere,

$$(n+1/2)\lambda_\ell = 2\pi a. \tag{9b}$$

Since $\lambda_\ell = 2\pi c_\ell/\omega$, this leads to

$$(n+1/2)\ c_\ell/c = ka, \tag{9c}$$

showing that the ratio of surface wave speed to sound speed in the external fluid can be obtained from reading off the ka-difference of adjacent resonance features caused by the lth surface wave in the form function:

$$c_\ell/c = \Delta(ka)_{n\ell}. \tag{9d}$$

With c = 1482m/c assumed in Fig. 1, this leads to an average speed of the Rayleigh wave in the vicinity of the ka=14.07 resonance (note its dispersion!) of c_ℓ = 4366 m/s, or to a step-width of $\Delta\tau$ = 2.13, in perfect agreement with Fig. 7.

V. Conclusions

We have performed a numerical study, accompanied by a physical interpretation, on the backscattering by a solid elastic sphere of finite-length sinusoidal acoustic wave trains, chosen of sufficiently long duration so as to permit the selective excitation of a given resonant vibration of the sphere. While the scattering of short pulses has previously been shown[10-12] to produce a sequence of individual, well-separated scattered pulses due to reflected and multiply-circumnavigating surface waves, it is seen here that long-pulse scattering leads similarly to a sequence of overlapping, long reflected and surface wave trains which give rise to several types of interference phenomena, to wit:

(a) At a resonance frequency, the succession of multiply-circumnavigating pulses builds up in phase, but interferes with the preceding reflected pulse mainly destructively (typically, for metal targets). We obtain a picture of an initially square reflected pulse, which due to these initial transients builds down step-wise to a quasi-stationary, reduced amplitude value. (If the interference with the reflected wave were constructive, this being the case for some Whispering-Gallery waves in metals, and more generally for light-weight targets such as lucite, a build-up to an augmented quasi-stationary amplitude value would occur; this was observed by Hickling[2]).

(b) Still at resonance, after the termination of the reflected pulse a step-wise decaying tail of multiply-circumnavigating, constructively interfering surface waves is observed.

(c) Moving off resonance, the surface waves get out of phase and begin to interfere destructively, thus causing both the initial transients and the tail to disappear.

In a related development, we have been able to obtain contour diagrams of the form function modulus for spheres of various materials, plotted over the complex frequency plane, which dramatically exhibit the structure of complex poles and zeros of the given target and hence lead to a better understanding of the interference features in the form function when plotted vs. real frequencies.

The main accomplishment of this work lies, we believe, in a demonstration that with properly chosen incident pulses of long duration, we can selectively excite individual resonances of a target, and study their properties via their induced ringing. A physical explanation of how this ringing is synthesized by the repeated circumnavigations of the circumferential surface wave which causes the resonances has been provided. The feasibility and potential applications of this technique for an identification of submerged elastic targets via their resonance spectrum[8-14] have been convincingly demonstrated in the experiments of Ripoche et al.[6-8]

Portions of this work were reported[23] at the Meeting of the Acoustical Society of America, San Diego, CA, November 1983. An analogous study for the case of radar scattering has also been performed by us[24].

Acknowledgements

One of the authors (H.Ü.) acknowledges most fruitful discussions with Drs. J. Ripoche, A. Derem, G. Maze, and J. L. Rousselot during a visit to their respective laboratories. He is also indebted to Drs. J. A. Bucaro and L. R. Dragonette for their hospitality and support at the Naval Research Laboratory, Washington, DC 20375.

Table I

Material parameters for elastic spheres

Material	ρ (g/cm^3)	c_ℓ (m/sec)	c_s (m/sec)
Tungsten Carbide	13.8	6960	4195
Aluminum	2.7	6370	3120
Lucite	1.182	2680	1380

References

1. J. J. Faran, J. Acoust. Soc. Amer. 23, 405 (1951).
2. R. Hickling, J. Acoust. Soc. Amer. 34, 1582 (1962).
3. A. J. Rudgers, J. Acoust. Soc. Amer. 45, 900 (1969).
4. N. Veksler, Information Analysis in Hydroelasticity, Academy of Sciences of the Estonian SSR, Institute of Cybernatics, Tallinn-Valgus, 1982.
5. G. C. Gaunaurd, E. Tanglis, H. Überall, and D. Brill, Nuovo Cimento 76B, 153 (1983); 77B, 73 (1983).
6. G. Maze, B. Taconet, and J. Ripoche, Phys. Lett. 84A, 309 (1981); Revue du CETHEDEC 72, 103 (1982).
7. G. Maze and J. Ripoche, J. Acoust. Soc. Amer. 73, 41 (1983); *Revue Phys. Appl.* 18, 319 (1983); *Proceed.* 11th International Congress on Acoustics, Paris, 1983.
8. A. Derem, J. L. Rousselot, G. Maze, J. Ripoche, and A. Faure, Acustica 50, 39 (1982); A. Derem, Revue du CETHEDEC 58, 43 (1979).
9. S. K. Numrich, L. R. Dragonette, and L. Flax, in Elastic Wave Scattering and Propagation, V. K. Varadan and V. V. Varadan, eds., Ann Arbor Science, 1982.
10. H. Überall and G. C. Gaunaurd, Appl. Phys. Letters 39, 362 (1981).
11. H. Überall, G. C. Gaunaurd, and J. D. Murphy, J. Acoust. Soc. Amer. 72, 1014 (1982).
12. G. C. Gaunaurd, H. Überall and A. Nagl, Proc. IEEE 71, 172 (1983).

13. H. Überall and G. C. Gaunaurd, Trans. IEEE Antennas Propag. (in press).

14. See, e.g., D. Brill, G. C. Gaunaurd, and H. Überall, J. Acoust. Soc. Amer. 72, 1067 (1982).

15. See, e.g., G. C. Gaunaurd and H. Überall, J. Acoust. Soc. Amer. 73, 1 (1983).

16. W. E. Howell and H. Überall, Trans. IEEE Antennas Propag. (in press).

17. W. E. Howell, Ph.D. thesis, Catholic University of America, 1984.

18. See, e.g., L. Flax, L. R. Dragonette, and H. Überall, J. Acoust. Soc. Amer. 63, 723 (1978).

19. A. Nagl, H. Überall, and K. B. Yoo, "Acoustic Exploration of Ocean Floor Properties Based on the Ringing of Sediment Layer Resonances", Technical Report, Nov. 30, 1983, Catholic University of America, Washington, DC 20064; submitted for publication to Journal of Geophysical Research B.

20. W. G. Neubauer, R. H. Vogt, and L. R. Dragonette, J. Acoust. Soc. Amer. 55, 1123 (1974).

21. See, e.g., J. J. Bowman, T. B. A. Senior, and P. L. E. Uslenghi, Electromagnetic and Acoustic Scattering by Simple Shapes, North-Holland, Amsterdam 1969.

22. See, e.g., L. Flax, G. C. Gaunaurd, and H. Überall, "Theory of Resonance Scattering", in Physical Acoustics vol. 15 (W. P. Mason and R. N. Thurston, eds.), Academic Press, New York, 1961, p. 191.

23. S. K. Numrich, W. E. Howell, and H. Überall, "Selective observation of elastic body resonances by using long pulses to excite a ringing response in the body", J. Acoust. Soc. Amer. 74, S108 (1983).

24. W. E. Howell and H. Überall, "Selective observation of resonances via their ringing in transient radar scattering", IEEE Trans. Antennas Propagat. 1984 (submitted).

Figure captions

Fig. 1. Form function modulus $|f(x)|$ plotted vs. real frequencies (top), and as a contour plot over complex frequencies (bottom), for tungsten carbide (c=1482m/s).

Fig. 2. Form function modulus $|f(x)|$ plotted vs. real frequencies (top), and as a contour plot over complex frequencies (bottom), for aluminum (c=1482 m/s).

Fig. 3. From function modulus $|f(x)|$ plotted vs. real frequencies (top), and as a contour plot over complex frequencies (bottom), for lucite (c = 1482 m/s).

Fig. 4. Enlarged portion of Fig. 1 (tungsten carbide) with c = 1482 m/s, showing one Rayleigh and one Whispering-Gallery pole.

Fig. 5. Top: spectrum of incident wave train superimposed on the form function of a tungsten carbide sphere; center: incident wave train; bottom: scattered pulse. Carrier frequency coincides with Rayleigh-wave interface dip at x_o = 14.07 in the form function.

Fig. 6. Same as Fig. 5, but with carrier frequency at x_o = 13.7, not coinciding with any resonance frequencies.

Fig. 7. Enlarged portions of the initial transient region (top) and final tail region (bottom) of Fig. 5, showing staircase effect.

Fig. 8. Schematic view of superposition (without any coherent or incoherent additions) of specular (large solid rectangle), penetrating and multiply internally reflected (dotted rectangles), and circumferential wave trains (small solid

rectangles), showing initial transient region (i), quasi- steady-state region (ii), and final transient region, or ringing (iii).

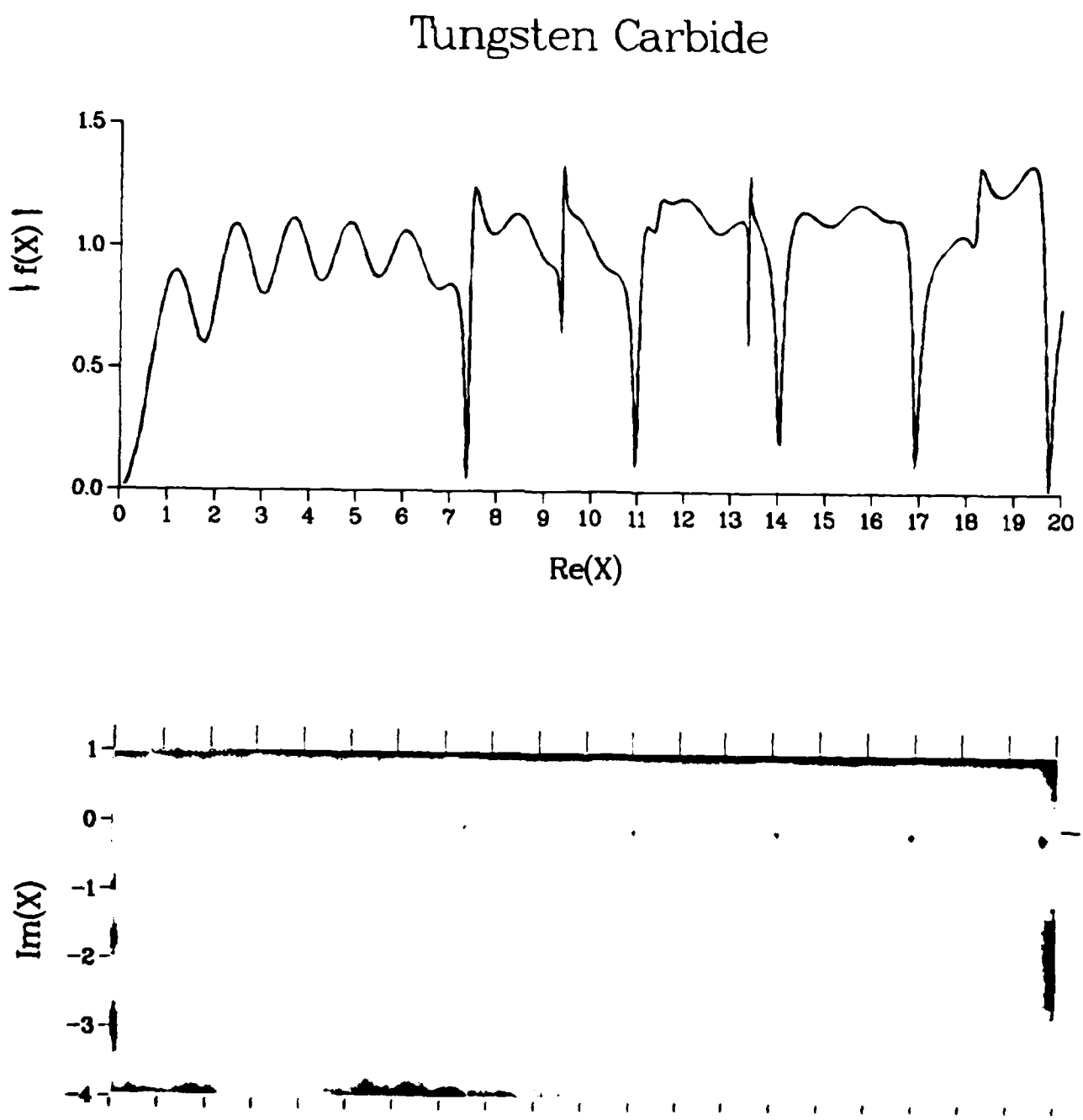
Tungsten Carbide
| f(X) |
1.5
1.0
0.5
0.0
0 1 2 3 4 5 6 7 8 9 10 11 12 13 14 15 16 17 18 19 20
Re(X)
Im(X)
1
0
-1
-2
-3
-4

Aluminum

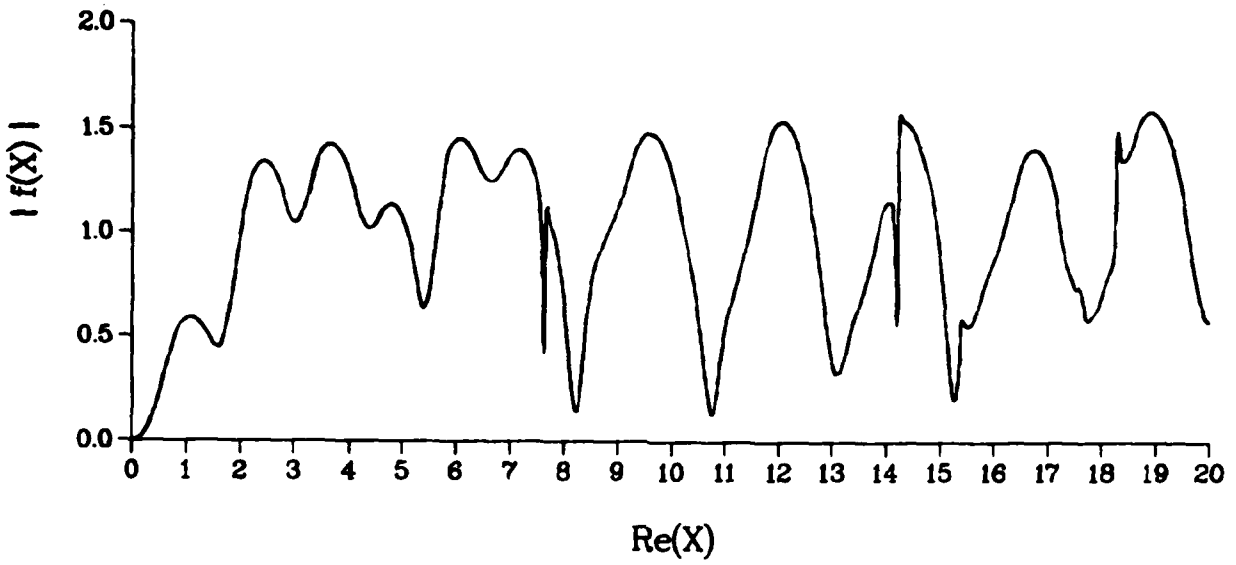
2.0
1.5
1.0
0.5
0.0
| f(X) |
0 1 2 3 4 5 6 7 8 9 10 11 12 13 14 15 16 17 18 19 20
Re(X)

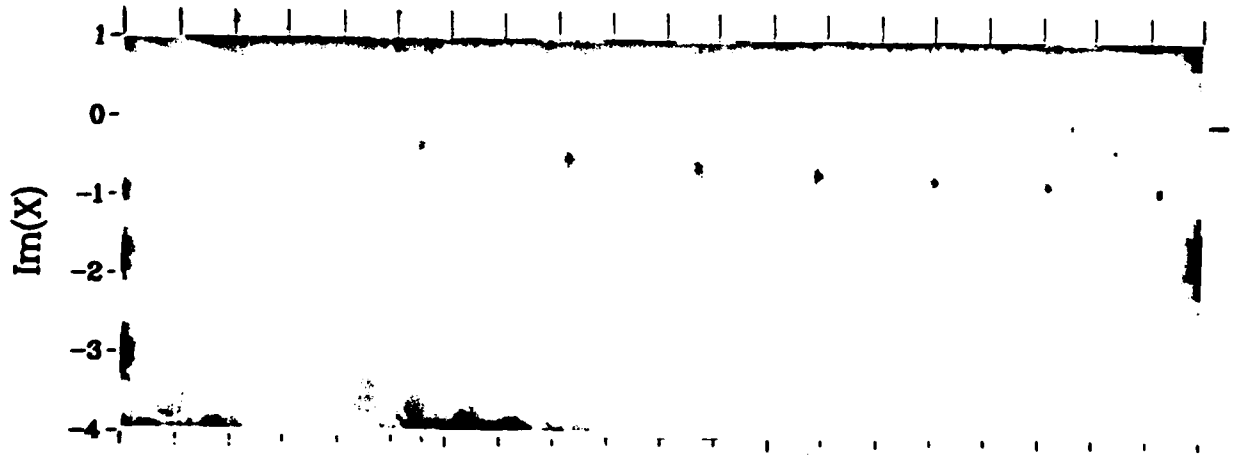
1
0
-1
-2
-3
-4
Im(X)

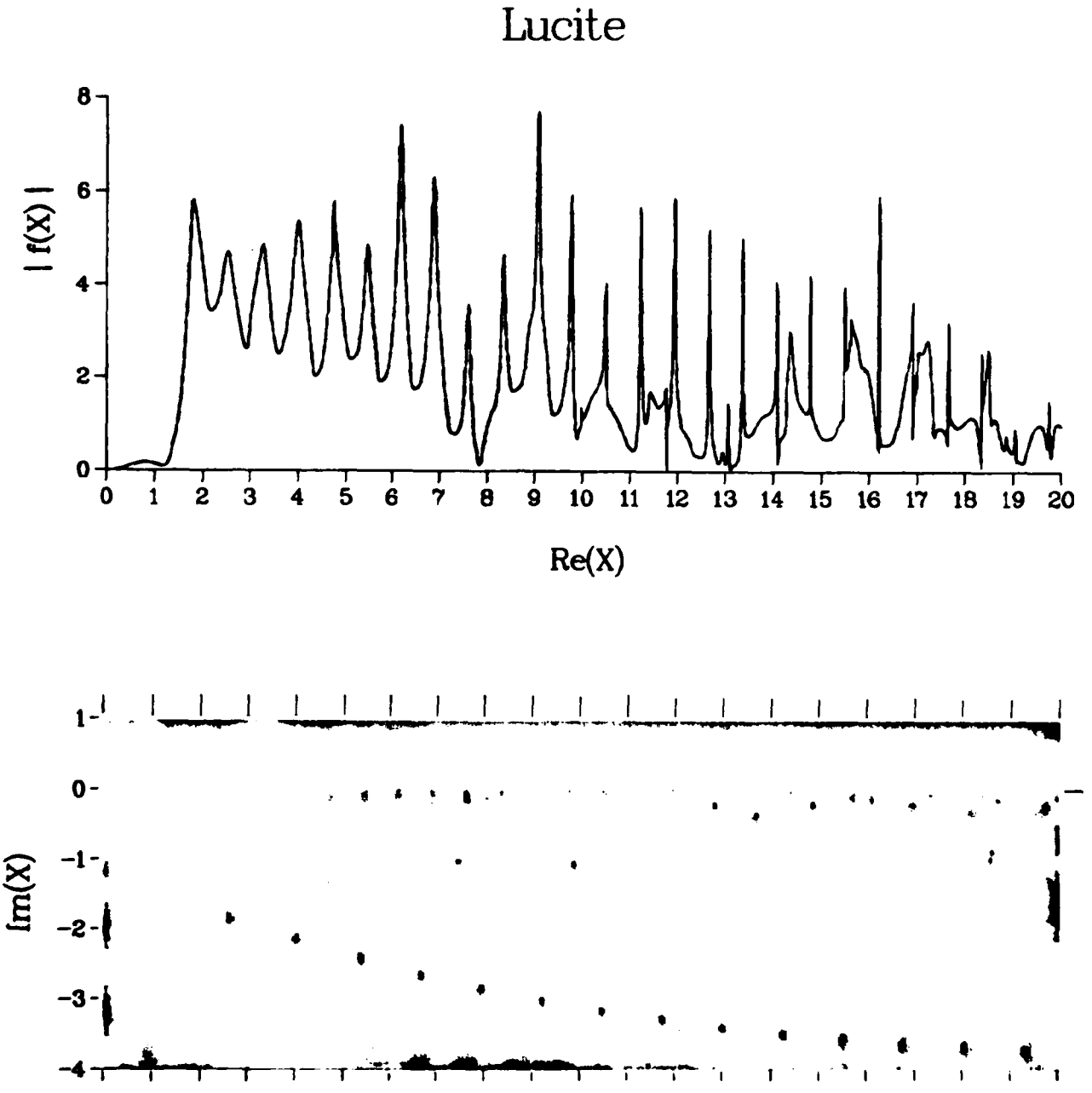
Lucite
| f(X) |
Re(X)
Im(X)

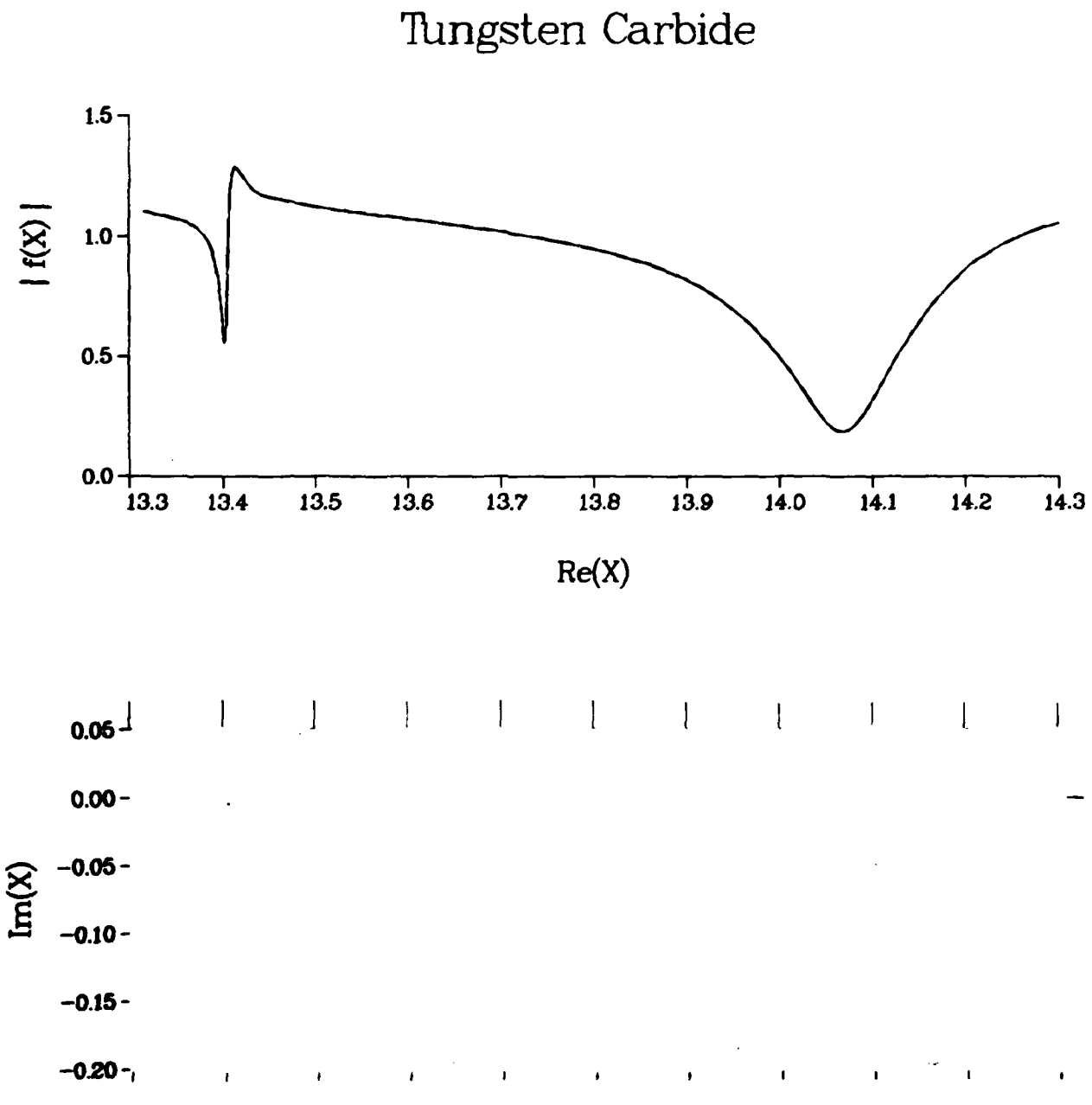
Tungsten Carbide
| f(X) |
1.5
1.0
0.5
0.0
13.3
13.4
13.5
13.6
13.7
13.8
13.9
14.0
14.1
14.2
14.3
Re(X)
Im(X)
0.05
0.00
-0.05
-0.10
-0.15
-0.20

Fig. 5

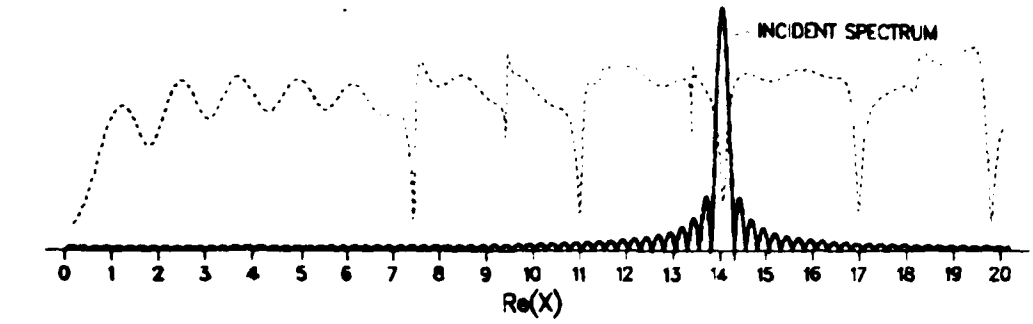
INCIDENT SPECTRUM
0 1 2 3 4 5 6 7 8 9 10 11 12 13 14 15 16 17 18 19 20
Re(X)

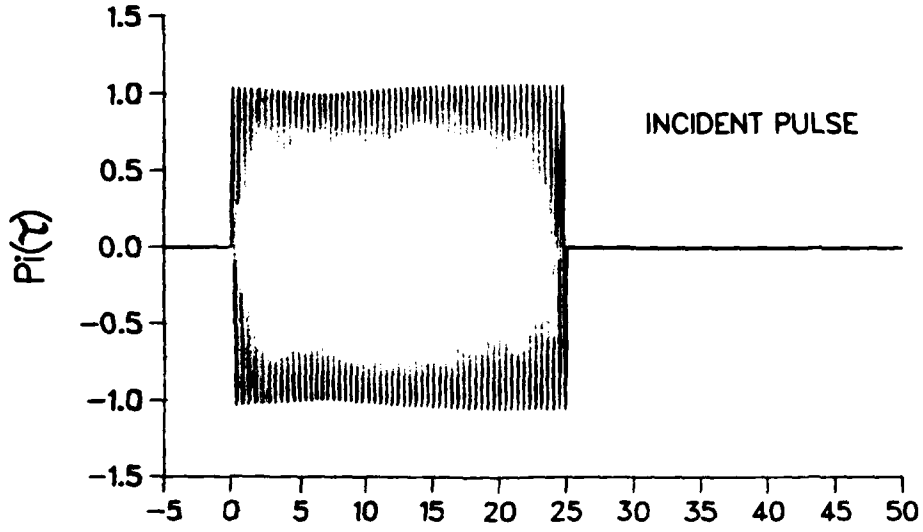
INCIDENT PULSE
Pi(τ)
1.5
1.0
0.5
0.0
-0.5
-1.0
-1.5
-5 0 5 10 15 20 25 30 35 40 45 50

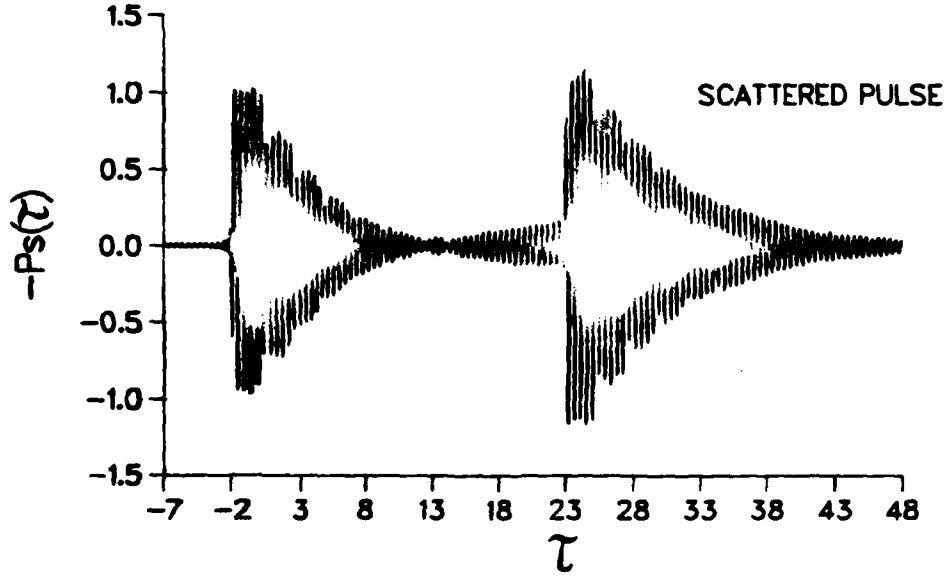
SCATTERED PULSE
-Ps(τ)
1.5
1.0
0.5
0.0
-0.5
-1.0
-1.5
-7 -2 3 8 13 18 23 28 33 38 43 48
τ

Fig. 6

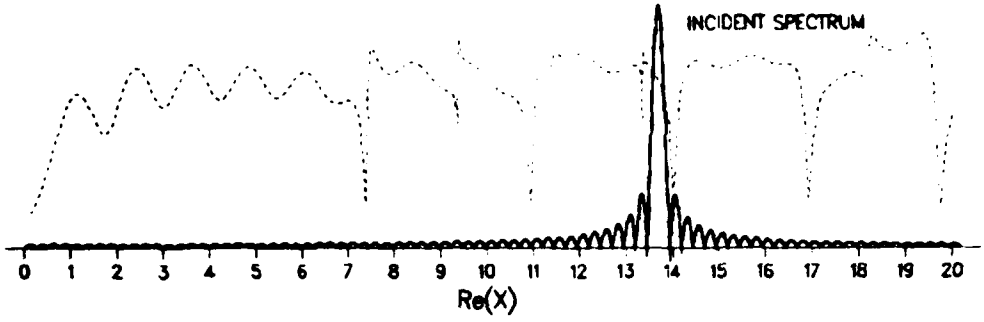
INCIDENT SPECTRUM
0 1 2 3 4 5 6 7 8 9 10 11 12 13 14 15 16 17 18 19 20
Re(X)

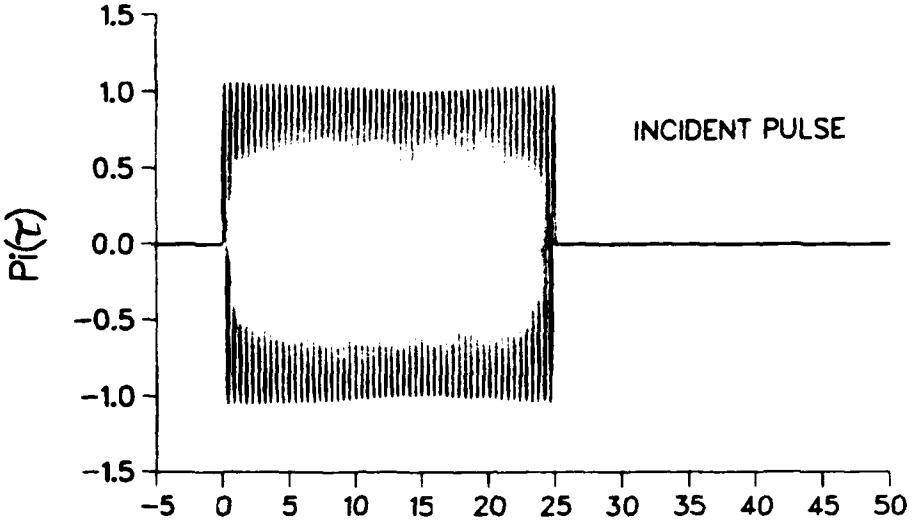
INCIDENT PULSE
Pi(τ)
1.5
1.0
0.5
0.0
-0.5
-1.0
-1.5
-5 0 5 10 15 20 25 30 35 40 45 50

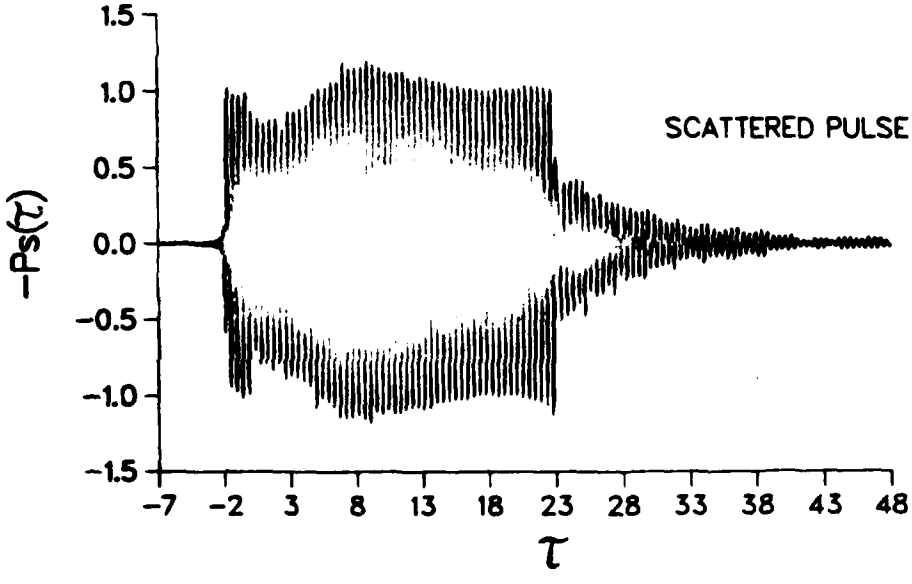
SCATTERED PULSE
-Ps(τ)
1.5
1.0
0.5
0.0
-0.5
-1.0
-1.5
-7 -2 3 8 13 18 23 28 33 38 43 48
τ

Fig. 7

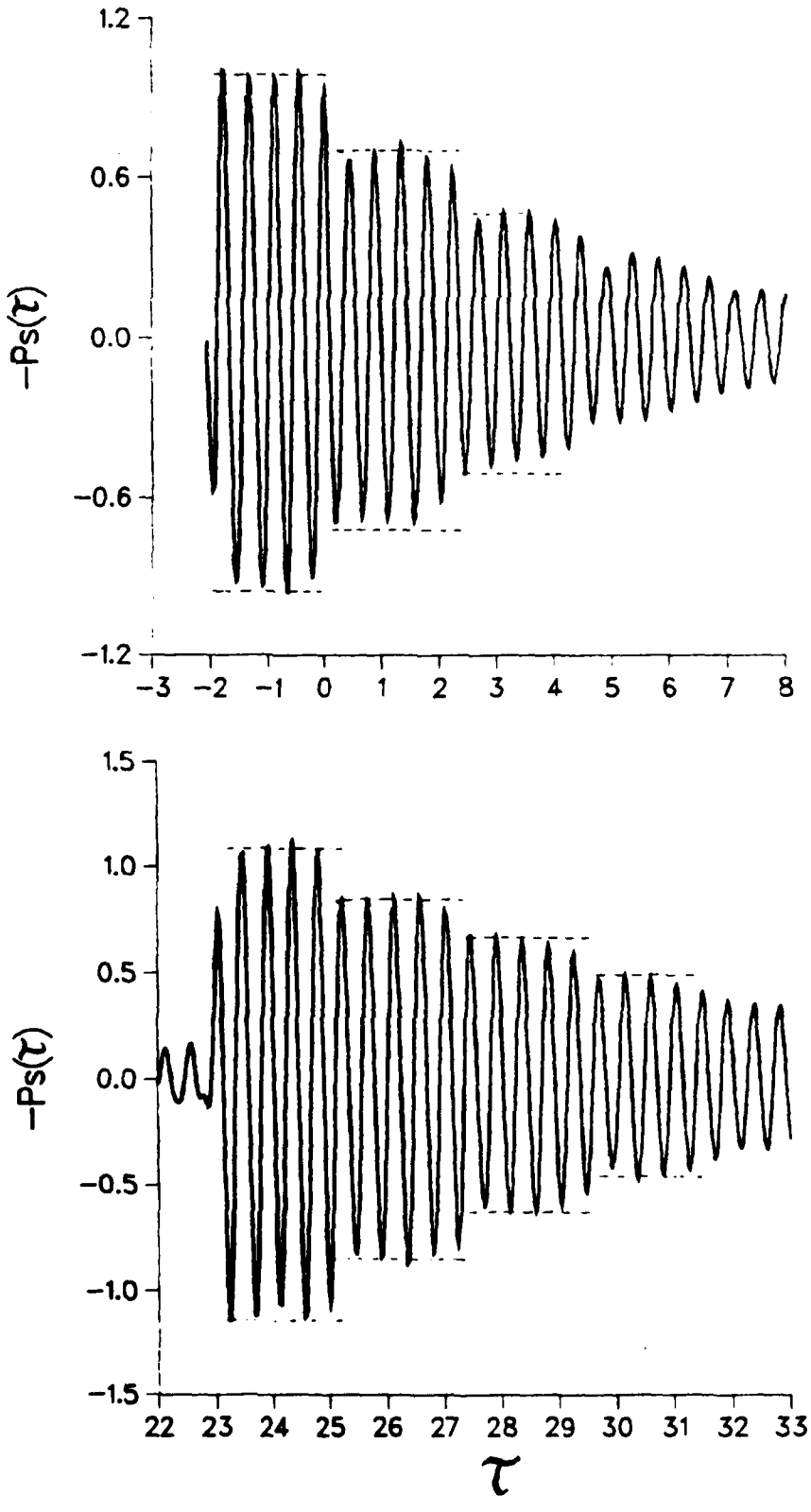
1.2
0.6
0.0
−0.6
−1.2
−Ps(τ)
−3 −2 −1 0 1 2 3 4 5 6 7 8
1.5
1.0
0.5
0.0
−0.5
−1.0
−1.5
−Ps(τ)
22 23 24 25 26 27 28 29 30 31 32 33
τ

Fig. 8